

The crystallography beamline I711 at MAX II

Y. Cerenius,^{a*} K. Ståhl,^b L. A. Svensson,^a T. Ursby,^a Å. Oskarsson,^c J. Albertsson^d and A. Liljas^a

^aDepartment of Molecular Biophysics, Center for Chemistry and Chemical Engineering, Lund University, PO Box 124, S221 00 Lund, Sweden, ^bDepartment of Chemistry, Technical University of Denmark, DK2800 Lyngby, Denmark, ^cDepartment of Inorganic Chemistry 1, Center for Chemistry and Chemical Engineering, Lund University, PO Box 124, S221 00 Lund, Sweden, and ^dDepartment of Inorganic Chemistry, Chalmers University of Technology, S412 96 Göteborg, Sweden. E-mail: yngve.cerenius@mbfys.lu.se

(Received 13 October 1999; accepted 7 April 2000)

A new X-ray crystallographic beamline is operational at the MAX II synchrotron in Lund. The beamline has been in regular use since August 1998 and is used both for macro- and small molecule diffraction as well as powder diffraction experiments. The radiation source is a 1.8 T multipole wiggler. The beam is focused vertically by a bendable mirror and horizontally by an asymmetrically cut Si(111) monochromator. The wavelength range is 0.8–1.55 Å with a measured flux at 1 Å of more than 10^{11} photons s^{-1} in 0.3 mm × 0.3 mm at the sample position. The station is currently equipped with a Mar345 imaging plate, a Bruker Smart 1000 area CCD detector and a Huber imaging-plate Guinier camera. An ADSC 210 area CCD detector is planned to be installed during 2000.

Keywords: X-ray crystallography; beamlines; MAX-lab.

1. Introduction

X-ray crystallography is a rapidly growing field. For example, Cambridge Structural Database (Allen, 1998) now includes almost 200 000 entries on organic, organometallic and metal complexes and the number of structures deposited in the Protein Data Bank (Bernstein *et al.*, 1977) has shown an almost exponential growth rate during the last years. The reasons for this are many and diverse. Changes in both experimental and computational crystallographic techniques coupled to advances in organic, inorganic and macromolecular preparation methods have, for example, allowed rather unstable molecules to be crystallized and very rare proteins to be produced in usable amounts, enhancing the scope of the crystallographic investigations. Moreover, the high brilliance of X-ray beams from synchrotron sources can be utilized to decrease the sample size both for small inorganic and large biological molecules. This allows increasingly difficult structural problems to be investigated by X-ray diffraction. Furthermore, short exposure times have made kinetic studies of rapid reactions feasible. This has created great demands and has put pressure on synchrotron sources all around the world to make high-quality X-ray crystallographic beamlines available. A beamline for use in the hard X-ray region has been built at the new MAX II storage ring in Lund, Sweden. MAX II is a third-generation 1.5 GeV storage ring (Table 1) dedicated to a wide variety of scientific studies using synchrotron light. MAX II is both a successor and complement to the older 500 MeV MAX I ring which has

Table 1

Parameters of the MAX II storage ring.

Parameter	Value	Units
Storage-ring energy	1.5	GeV
Current	200–250	mA
Ring circumference	90	m
Number of straight sections	10†	
Straight-section length	3.2	m
Radio frequency	500	MHz
Horizontal emittance	8.8×10^{-9}	rad m

† Eight straight sections can be used for insertion devices.

been in operation since 1986 (Andersson *et al.*, 1994) and where the radiation energy at the beamlines is in the UV and soft X-ray regime. The crystallographic beamline, I711, is designed for macromolecular, small-molecule and powder crystallography. The beamline has been in scheduled use since August 1998. The results obtained so far at I711 show that a high-quality X-ray crystallographic beamline can be built at third-generation storage rings having relatively low ring energies.

2. The I711 insertion device

Beamline 711 is placed on a multipole wiggler insertion device, built by VTT Automation in Esbo, Finland. The magnets are of a permanent field type with a peak field of 1.8 T. The characteristic wavelength of the wiggler is 4.6 Å.

Table 2
I711 wiggler parameters.

Parameter	Value	Units
Total length	2.65	m
K_{\max}	29.3	
Magnetic gap	23–300	mm
Period	174	mm
Number of poles	27	
Critical photon energy	2.69	keV
Calculated flux at 15 keV	1.5×10^{12}	photons s^{-1} (0.1% bandwidth) $^{-1}$
Total power	2.21	kW
Power into 3 mrad \times 0.3 mrad	0.26	kW
Central power density	0.28	kW mrad 2

At 0.8 Å the calculated flux is 1.5×10^{12} photons s^{-1} (0.1% bandwidth) $^{-1}$ (see Table 2 for more wiggler parameters). A comparison of the calculated source flux between the wiggler of this beamline and two other crystallographic beamlines, *e.g.* the three-pole 5 T superconducting wiggler at station 9.6 at Daresbury (Helliwell *et al.*, 1986) and a 0.8 T bending-magnet beamline at the ESRF (ESRF

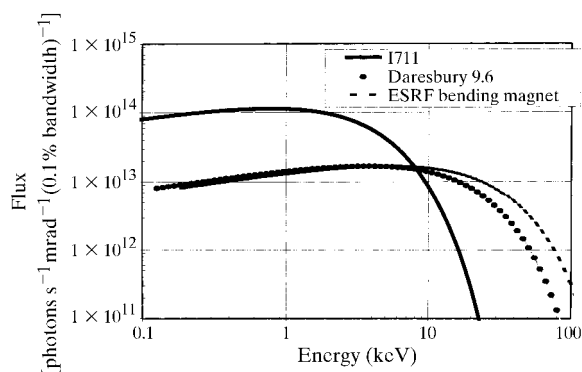


Figure 1
Source flux comparison between the wiggler at I711, the superconducting wiggler at station 9.6 at Daresbury and a bending-magnet beamline at the ESRF.

Beamline Handbook, 1993), is presented in Fig. 1. As seen from the plot, the flux at I711 is quite comparable at energies below 10 keV (wavelength longer than 1.2 Å) but decreases significantly faster towards higher energies. MAX II has a lower energy of the stored beam, 1.5 GeV compared with 6 GeV at the ESRF. Moreover, the magnetic field of the wiggler at station 9.6 at Daresbury is three times as strong as that at I711. Therefore the high-flux region is pushed towards higher energies for the two other beamlines [since the critical energy is proportional to the magnetic field and to the square of the storage-ring energy (Freund, 1993)], while I711 is superior at longer wavelengths.

3. Beamline layout

An illustration of the design of beamline 711 is given in Fig. 2. It is to a large extent a copy of station 9.6 at the SRS Daresbury, UK (Helliwell *et al.*, 1986). Daresbury Laboratory was also involved in the initial calculations comparing possible insertion devices. Station 9.6 is dedicated to high-intensity protein crystallography and a decision was taken to use its well established design to minimize the time for obtaining a fully operational crystallographic beamline at the MAX-laboratory. Most of the drawings for I711, based on station 9.6, were therefore purchased from Daresbury Laboratory.

3.1. Front end

An adjustable aperture with a maximal opening of 3.4 mrad is situated 4.4 m from the centre of the straight section. Most of the power emitted from the wiggler is absorbed in a 2 mm-thick water-cooled Be window, separating the beamline from the storage-ring vacuum. This window cuts off all X-rays with wavelengths greater than 3 Å. The first component after the shield wall of the storage ring is a pair of water-cooled slits which, together with the aperture, determine the size of the radiated area on the mirror.

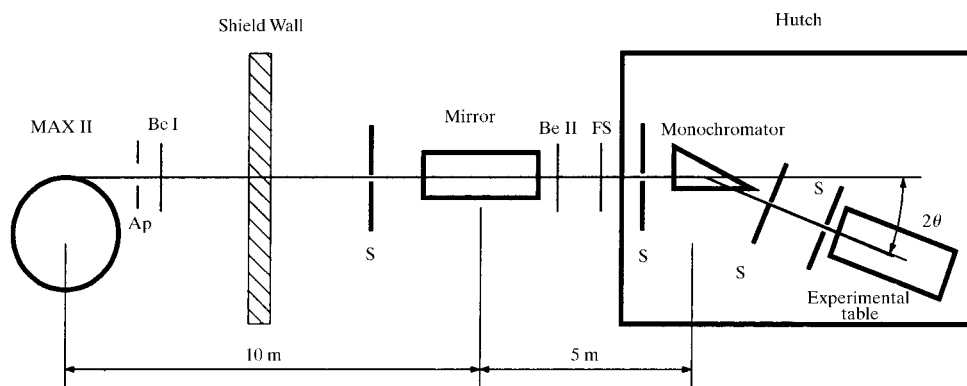


Figure 2
Schematic diagram of the beamline layout. Ap = aperture, Be I = water-cooled Be window, Be II = beryllium window, S = slits, FS = fluorescent screen.

3.2. Mirror

A focusing mirror is situated 10 m from the source. It consists of a 1200 mm-long, 95 mm-wide and 80 mm-thick glass rod coated with a minimum adhesive chromium layer followed by a 200 Å-thick platinum layer with a surface roughness of less than 10.0 Å RMS. The angle of incidence is normally set to 3 mrad, giving an energy cut-off of 30 keV, and thereby removing harmonics with wavelengths shorter than 0.4 Å. Higher incidence angles can be used for cut-off further up in wavelength. The mirror can be bent to focus the beam in the vertical direction with a minimum focal length of 7.0 m. The mirror was purchased from Photon Sciences International Inc., Tuscan, AZ, USA, and the mirror mechanism was supplied by CVT Ltd, Milton Keynes, UK. An almost identical mirror mechanism design is described by Cernik *et al.* (1997). No thermal problem has been observed with the mirror but an active damping system lead to severe stability problems and had to be replaced by a passive system. This replacement was possible because of the stable floor at the MAX II hall.

After the mirror a second beryllium window (0.25 mm-thick, without water cooling) is mounted. This separates the vacuum of the mirror chamber (10^{-8} mbar) from the downstream parts of the beamline (10^{-3} mbar). The next component is a fluorescent screen which can be inserted into the beam to study the direct beam or the beam deflected by the mirror. The image on the fluorescent screen is recorded by an external video camera through a viewing window (see Fig. 3).

3.3. Monochromator

The monochromator is located 15 m from the source and consists of a triangularly shaped Si(111) single crystal. The crystal is 290 mm long, 40 mm high (at the wide end) and 1.5 mm thick. It is clamped at the wide end to a similarly shaped Cu plate. The crystal with its support plate is cylindrically bent for horizontal focusing. The curvature is produced by a pin pressing the tapered end of the crystal. The crystal is asymmetrically cut (presently a crystal with an asymmetric angle of 7° is used) which compresses the

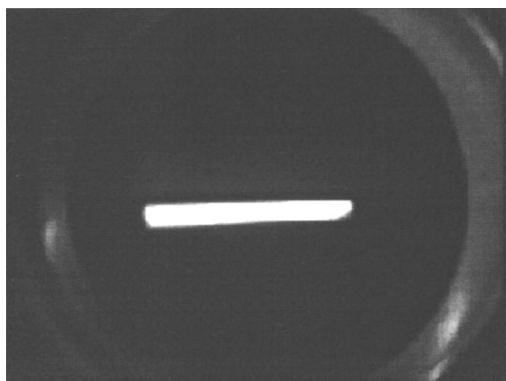


Figure 3
Fluorescent screen image of the beam reflected by the mirror. The beam size here is approximately 50 mm \times 5 mm.

reflected beam compared with the incident beam and shortens the focal distance (Helliwell, 1992). Two pairs of water-cooled slits are mounted upstream of the monochromator. The horizontal opening of these slits determines the width of the radiated part of the monochromator crystal and can be used to improve the wavelength resolution, at the expense of intensity. The monochromator reflects the X-ray beam in the horizontal plane which simplifies the mechanical design of the rest of the experimental set-up which has to follow the reflected beam as the wavelength is changed. The drawback of this design is the polarization loss primarily at longer wavelengths (Helliwell, 1992). The monochromator crystal is placed in a vacuum chamber (10^{-3} mbar) and the crystal is brought into thermal contact with its supporting Cu plate by a thin layer of gallium. The crystal, together with the plate, is partly set in a bath of liquid Ga–In–Sn alloy situated in a water-cooled Cu block. The crystal and its block are mounted on three rotary stages (Newport Ltd, Newbury, UK) so that the 2θ angle can be changed as well as the pitch and tilt angles of the crystal. In addition, there is a possibility of adjusting the vertical position of the crystal with a stepper motor that is operating outside of the vacuum. Owing to the present mechanical set-up of the monochromator crystal holder, the upper wavelength limit is slightly above 1.54 Å. However, the design would allow the upper wavelength limit to be close to 2 Å. Another two pairs of slits are mounted between the monochromator and the experimental table. These slits are primarily used for defining the beam size, if a smaller size than the optimal focus is required. To minimize intensity losses due to scattering and absorption of the radiation in air, a tube with Mylar windows at both ends is mounted between the monochromator vessel and the experimental table. The length of the tube can be varied between 0.4 and 6 m. The tube is evacuated by a rotary pump ensuring a vacuum of 10^{-2} mbar or better. The last pair of slits before the sample are closed as much as possible to reduce the amount of scattered radiation from the previous slits.

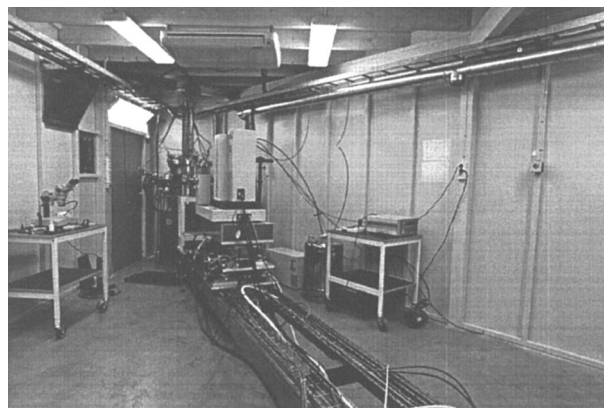


Figure 4
A photograph from the inside of the hutch showing the monochromator vessel, the 2θ arm with the experimental table and an image-plate detector with a cryosystem mounted.

3.4. 2θ arm and experimental table

Besides the monochromator vessel, the experimental hutch encloses the 2θ arm and the experimental table (Fig. 4). Owing to the monochromator design, the experimental table has to be moved when the energy is changed (see Fig. 2). The experimental table is mounted on the 2θ arm which is motorized and has a 2θ range of $0\text{--}40^\circ$. The table can be translated along the 2θ arm so that the distance between the monochromator and the sample is 1–6 m, corresponding to optimal focusing for $0.85\text{--}1.7\text{ \AA}$ (for a monochromator crystal with an asymmetry angle of 7°). The experimental table also has motorized adjustments for translations and rotations in the vertical and horizontal directions. For a trained operator it takes, at most, half an hour to change the wavelength and to optimize the beam at the new position. However, small changes in wavelength can be performed more rapidly.

4. Radiation properties

4.1. Intensity

The absolute intensity of the X-ray beam has been measured at the sample position with a semiconducting diode (Hamamatsu S3590, Hamamatsu City, Japan) as a function of the wavelength. The beam was collimated to $0.3\text{ mm} \times 0.3\text{ mm}$. The diode was tested both with and without a negative bias (up to 40 V), to increase the depletion depth. No significant differences were observed between the measurements. At wavelengths above 1 \AA the intensity was measured to be greater than 10^{11} photons s^{-1} . The source flux from the wiggler increases with wavelength. However, Fig. 5 shows the intensity that an experimentalist at the beamline would obtain at a certain wavelength. The measured signal from the diode has thus been corrected for

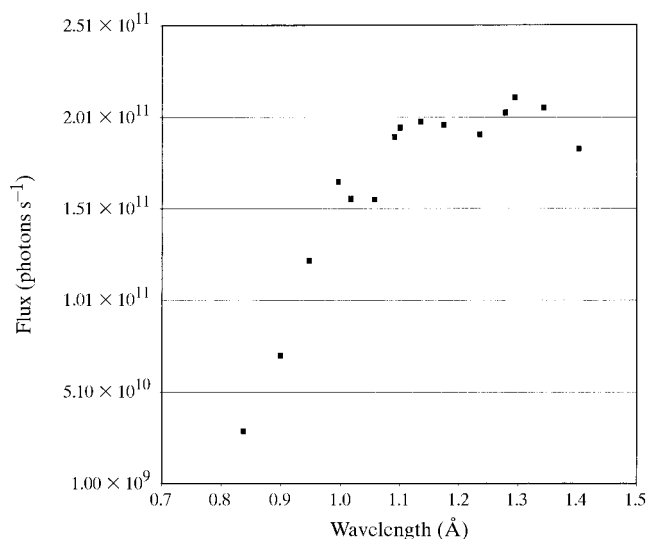


Figure 5 Absolute intensity at the sample position as a function of wavelength.

the absorption in the aluminium foil surrounding the silicon chip and for the finite absorption in the chip, but it has not been corrected for other losses which are always present. These losses include the absorption between the monochromator and the sample (in the Be and the Mylar foils as well as in the residual gas in the evacuated tube along the 2θ arm and in the minimized air path). The distance along the 2θ arm differs with wavelength and therefore also with the length of the evacuated tube. The length of the air path also depends on the wavelength since the tube length is determined by the lengths of a fixed number of pre-made tubes and it is therefore not always possible to match the tube length with an optimal focusing distance. Moreover, loss in intensity due to absorption (in the Be and Mylar windows of the beamline) and polarization from the monochromator decrease the slope of the curve at wavelengths above 1.1 \AA , seen in Fig. 5.

4.2. Spot size

The focusing power of the beamline is determined by the bending of the monochromator and the mirror. In addition, the asymmetrically cut monochromator crystal helps to compress the diffracted beam horizontally, especially at shorter wavelengths. The preferred spot size is, however, usually smaller than the focusing power of the beamline, and therefore the spot size is normally defined by the slits or by the collimator of the goniostat. In order to measure the focusing power of the beamline, all slits of the beamline were left wide open and an area-sensitive ionization detector by Artemiev *et al.* (1996) was placed at the sample position. At a wavelength of 1.3 \AA the spot size of the unfocused beam (flat monochromator and mirror) was measured to be $7\text{ mm} \times 2\text{ mm}$ (FWHM) while the spot size of the focused beam was measured to be $1.0\text{ mm} \times 0.5\text{ mm}$ corresponding to a demagnification of about 30. Fig. 6 shows the spot sizes using an unfocused monochromator

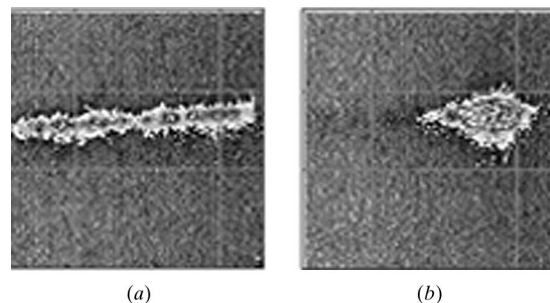


Figure 6 Images of the X-ray beam at the sample position collected with an area-sensitive ionization detector at a wavelength of 1.3 \AA . The first photograph (a) was taken with an unfocused monochromator and a focused mirror showing a spot size of $7\text{ mm} \times 0.5\text{ mm}$ (FWHM). In the second photograph (b), both the mirror and monochromator are focused. The spot size is here $1\text{ mm} \times 0.5\text{ mm}$ (FWHM).

and a focused mirror, and then using a focused monochromator and a focused mirror.

5. Software

All hardware at the beamline, except for the detectors, are controlled by two PCs. Control of the front end, heat absorbers and gauges is *via* one PC running the *Intouch* software package from Wonderware Inc., Irvine, CA, USA, connected to a PLC (programmable logical controller, Allen-Bradley SLC500, from Rockwell Inc., Milwaukee, WI, USA), through a com-port. The PLC system also contains logics to protect the users and the hardware and can also read analogue signals, *i.e.* temperatures. Alarm temperatures for the motors inside the evacuated monochromator vessel and cooling water temperatures from slits along the beamline are set by the software. The second PC controls the optics (mirror, monochromator and slits) as well as the position of the experimental table. In all, 32 different stepper motors are used to position the items. The software, developed at the beamline, is written in Fortran and communicates with the controllers from Mclennan Ltd, Camberley, UK. Many of these motors work in pairs (*i.e.* moving a pair of slits) and are therefore defined as virtual motors in the interface to make the software more user friendly. Pulses from semiconducting diodes or ionization chambers are used during motor scans for beam intensity optimization.

6. Detectors

The following apparatus are currently available at the beamline:

(i) A Smart 1000 CCD from Bruker AXS Inc., Madison, WI, USA, for small-molecule crystallography and powder diffraction with a 90 mm-diameter active area and 1024×1024 pixels. The detector is equipped with a three-circle fixed- χ goniometer, a rotary shutter for fast exposures, collimators down to 50 μm for small beam sizes and software packages for on-site analysis of both powder and single-crystal data.

(ii) A Marresearch 345 imaging plate from X-ray Research GmbH, Norderstedt, Germany, with up to 345 mm-diameter of active area. The detector is equipped with an extended base with a maximum crystal-to-detector distance of 770 mm and is suitable for macromolecular crystallography. The turnover time varies between 34 and 108 s depending on chosen readout diameter and resolution.

(iii) A Huber (Huber Diffraktionstechnik GmbH, Rimsting, Germany) Image Foil Camera 670 with both a flat specimen and capillary holder is used for powder diffraction experiments (Stahl, 2000).

(iv) Installation of a 2×2 CCD detector with fast readout (Quantum 210, ADSC, Poway, CA, USA) is

planned for 2000 and will be used mainly for macromolecular crystallography.

These detectors can fairly easily be changed to ensure the users the possibility for all types of experiments for which the beamline was built. Because of the polarization of the synchrotron beam, the SMART detector is mounted so that the 2θ axis is horizontal instead of vertical. The same will be true for the Quantum 210 system.

All experimental set-ups can be equipped with a Cryostream from Oxford Cryosystems Ltd, Oxford, UK, for low-temperature data collection. A Huber sample heater device particularly for powder-diffraction experiments is also available. The experiments are controlled from a separate data-acquisition cabin. In addition, the beamline has facilities for preparation both at cold and ambient temperatures and a computer room for on-site data analysis. Moreover, a chemical laboratory is available at the MAX-laboratory.

7. Applications and results

The first diffraction data were collected in May 1997 and the first macromolecular structure was solved by the multiple isomorphous replacement (MIR) method from data collected at I711 in June of the same year (Unge *et al.*, 1998). The commissioning period ended in July 1998 and the beamline is now fully operational and open for users through proposals addressed to the MAX-laboratory. Approximately 30 user groups are allocated beam time at I711 per year.

More information about the beamline can be found at <http://www.maxlab.lu.se/beamlines/bli711/mainpage.htm>.

The Swedish Council for Planning and Coordination of Research, FRN, and the Swedish Natural Science Research Council, NFR, are acknowledged for funding of the beamline. The Knut and Alice Wallenberg Foundation is acknowledged for funding of the Quantum 210 detector system. The staff at MAX-lab are thanked for their help in building the beamline and for the supply of photons. Dr Colin Nave and colleagues at Daresbury Laboratory for production and modifications of the original drawings and Dr Howard Padmore for wiggler beam simulations and evaluations are also thanked.

References

- Allen, F. H. (1998). *Acta Cryst.* **A54**, 758–771.
- Andersson, Å., Eriksson, M., Lindgren, L.-J., Röjssel, P. & Werin, S. (1994). *Nucl. Instrum. Methods Phys. Res. A*, **343**, 644–649.
- Artemiev, A. N., Ioudin, L. I., Lightenshtein, V. H., Mikhailov, V. H., Peredkov, S. S., Rakhimbabaev, T. Y., Rezvov, V. A., Sklyarenko, V. I., Lemonnier, M., Megert, S. & Roulliy, M. (1996). In *Proceedings of the Fifth European Particle Accelerator Conference (EPAC96)*, Vol. 2. Bristol: IOP Publishing.
- Bernstein, F. C., Koetzle, T. F., Williams, G. J., Meyer, E. E. Jr, Brice, M. D., Rodgers, J. R., Kennard, O., Shichi, T. & Tasumi, M. (1977). *J. Mol. Biol.* **112**, 535–542.

- Cernik, R. J., Clegg, W., Catlow, C. R. A., Bushnell-Wye, G., Flaherty, J. V., Greaves, G. N., Burrows, I., Taylor, D. J., Teat, S. J. & Hamichi, M. (1997). *J. Synchrotron Rad.* **4**, 279–286.
- ESRF Beamline Handbook (1993). *ESRF Beamline Handbook D1 Swiss–Norwegian CRG*, pp. 17–20. ESRF, Grenoble, France.
- Freund, A. (1993). *X-ray Optics for Synchrotron Radiation from Neutron and Synchrotron Radiation for Condensed Matter Studies*, Vol. 1, *Theory, Instruments and Methods*. Berlin/Heidelberg: Springer-Verlag.
- Helliwell, J. R. (1992). *Macromolecular Crystallography with Synchrotron Radiation*, pp. 138–163. Cambridge University Press.
- Helliwell, J. R., Papiz, M. Z., Glover, I. D., Habash, J., Thompson, A. W., Moore, P. R., Harris, N., Croft, D. & Pantos, E. (1986). *Nucl. Instrum. Methods Phys. Res. A*, **246**, 617–623.
- Stähl, K. (2000). *J. Appl. Cryst.* **33**, 394–396.
- Unge, J., Åberg, A., Al-Kharadaghi, S., Nikulin, A., Nikonov, S., Davydova, N. L., Nevskaya, N., Garber, M. & A Liljas, A. (1998). *Structure*, **6**, 1577–1586.